Large field homogeneous illumination in microwave-induced thermoacoustic tomography based on a quasi-conical spiral antenna

An Yan, Li Lin, Shuai Na, Changjun Liu, and Lihong V. Wang

Citation: Appl. Phys. Lett. **113**, 123701 (2018); doi: 10.1063/1.5043541
View online: https://doi.org/10.1063/1.5043541
View Table of Contents: http://aip.scitation.org/toc/apl/113/12
Published by the American Institute of Physics

Large field homogeneous illumination in microwave-induced thermoacoustic tomography based on a quasi-conical spiral antenna

An Yan,[1,2] Li Lin,[2] Shuai Na,[2] Changjun Liu,[1,a)] and Lihong V. Wang[2,a)]
[1]*School of Electronics and Information Engineering, Sichuan University, Chengdu 610064, China*
[2]*Caltech Optical Imaging Laboratory, Andrew and Peggy Cherng Department of Medical Engineering, Department of Electrical Engineering, California Institute of Technology, Pasadena, California 91125, USA*

(Received 10 June 2018; accepted 7 September 2018; published online 21 September 2018)

Conventional helical and horn antennas based on frequency selective surfaces have been used to provide microwave illumination in microwave-induced thermoacoustic tomography (TAT). However, the electromagnetic waves radiated from the conventional antennas are not circularly polarized and thus impair image quality. In addition, conventional antennas can provide uniform radiations only within a relatively small area and thus limit their clinical applications (e.g., breast imaging). To address these problems, we propose a quasi-conical log-spiral antenna for homogenous illumination over a large field. We theoretically and experimentally validated this approach. Tissue-mimicking phantoms were imaged. The antenna produced not only an electric field with a circular polarization but also a homogeneous illumination area with a 10 cm diameter. Accordingly, our method has advanced TAT by improving microwave illumination. *Published by AIP Publishing.*
https://doi.org/10.1063/1.5043541

Microwave imaging provides high contrast in breast imaging, but the spatial resolution is limited.[1–3] Ultrasonography has been used as an adjunct to mammography but suffers from speckle artifacts. Light-induced photoacoustic tomography can offer a functional optical contrast in breast imaging; however, the penetration is limited to 4 cm.[4,5] Thermoacoustic tomography (TAT) combines the advantages of both microwave absorption contrast and ultrasound spatial resolution, providing deep penetration and complementary contrasts based on dielectric properties, which are found to be different between normal and malignant tissues.[6–9] Breast cancer has a higher microwave absorption coefficient than normal breast tissue (0.5–6 GHz), giving TAT a great potential for breast cancer imaging.[10,11] The 3-GHz microwave can provide a penetration depth of 1.2 and 9 cm in muscle and fat, respectively, which makes it suitable to detect breast tumor.[12]

When the size of an object is smaller than the microwave wavelength, we usually assume that the electric-field distribution in the object is uniform to simplify the computation. However, the influence of the field distribution cannot be ignored when the object is larger than the wavelength. Homogenous electric field distribution is preferred to reconstruct the microwave absorption coefficients.[13] Both the polarization mode and electric-field distribution of the microwave are determined by the antenna.[14] A rectangular waveguide has the simplest aperture and is the most common microwave transmitting device used in TAT.[15,16] There can be some sources of loss in a waveguide, such as radiative loss (in a bent waveguide) or scattering due to sidewall roughness, for instance. A horn antenna has a better direction coefficient and a lower reflectivity,[17–19] but the linearly polarized electric field produces misrepresentations in the reconstructed images.[20] The horn antennas based on frequency selective surfaces (FSSs) cannot realize circular polarizations.[21] A traditional helical antenna can produce elliptically polarized illumination,[22] especially when the size of the object is comparable to the microwave wavelength. The linearly polarized components in the electric field also cause image distortions or shadows. Most importantly, traditional antennas used for TAT can provide a uniform illumination field smaller than most human organs (e.g., breast). Accordingly, the reconstructed TAT images suffer misrepresentations.

Quasi-conical spiral antennas elicited much interest in wireless communications over the past decade. Conical spirals are chosen because they generally provide much wider bandwidths and higher circularly polarization than traditional helical antennas.[23–25] These advantages make conical spiral antennas well suited for TAT. Here, we propose a type of conical antenna, which produces a highly circularly polarized electric field with a uniform distribution over a large area. According to Rumsey's theory, the performance of a conical spiral antenna is defined entirely by angles, and the antenna must have an "active region" that is responsible for the radiation at a particular frequency.[26]

The conical spiral is modified from the equiangular spiral and can be mathematically expressed as follows:[27] As shown in Fig. 1, α and S denote the wrap angle and coil spacing, respectively. D denotes the bottom diameter of the conical spiral structure and d the top diameter. C denotes the circumference of a turn on the quasi-conical spiral antenna (Fig. 1). The wrap angle can be expressed as $\alpha = arc\tan(S/\pi D)$. The beam width of the radiation field depends on the main lobe and can be maximized by changing the wrap angle. The wrap angle is also adjusted to optimize the circular polarization over a wide angular range of radiation fields. We added a traditional helical structure to improve the radiation efficiency. S11 was improved from –8 dB to –17 dB at 3 GHz. We added a taper to eliminate the microwave coupling. The coil spacing S_P is set as 10 mm to optimize the circular polarization and gain (Fig. 3). The design process is shown in Fig. 2.

a)Authors to whom correspondence should be addressed: cjliu@scu.edu.cn and LVW@caltech.edu.

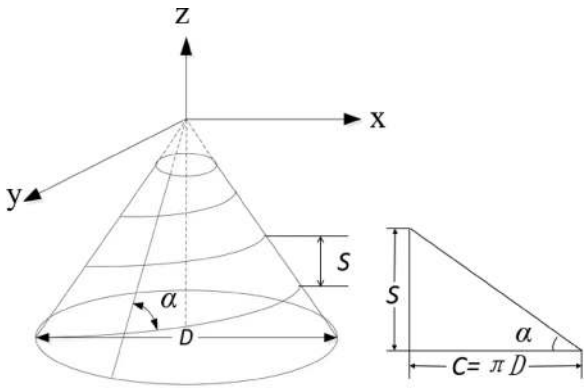

FIG. 1. The schematic of the conical logarithmic spiral structure.

After an iterative optimization, we created a quasi-conical spiral structure with parameters set as follows: $S = 14$ mm, $\alpha = 0.244$, $d = 2$ mm, and $D = 17.5$ mm (Fig. 3).

The bottom end of the quasi-conical spiral copper wire is connected to the coaxial inner conductor. A metal disk connecting to the ground is mounted at the end of the copper wire to eliminate the current in the outer skin of the coaxial line and form a current loop within the spiral. The metal disk also plays an important role in reducing reflection of the microwave and increasing the gain of the antenna. A traditional helical antenna was designed to compare with the quasi-conical spiral antenna in circular polarization purity and electric field distribution. The axial ratio is the ratio of orthogonal components of an E-field.[28] A circularly polarized field is made up of two orthogonal E-field components of equal amplitude (and 90° out of phase). Because the components are of an equal magnitude, the axial ratio is 1 (or 0 dB). The axis ratio is an important performance indicator describing the purity of circular polarization. A smaller axis ratio represents a higher polarization purity. Compared to the traditional helical antenna, the quasi-conical spiral antenna can produce a lower value of the axis ratio over a wider angular range (Fig. 4). Therefore, the circular polarization characteristic of the quasi-conical spiral antenna is much better than the traditional antenna.

An air layer with a relative dielectric constant of 1 and a relative magnetic permeability of 1 has been established for the simulation. We use a model with a diameter of 10 cm to mimic the normal size of the breast. Figure 5(a) shows the electric field distribution produced by the traditional helical antenna at the distance of 5 cm. Figure 5(b) shows the electric field distribution of the quasi-conical spiral antenna at the distance of 5 cm. The full width at half maximum (FWHM) of the traditional helical antenna is 10 cm. The FWHM of the quasi-conical antenna a is 15 cm. Obviously, the quasi-conical spiral antenna can produce a uniform

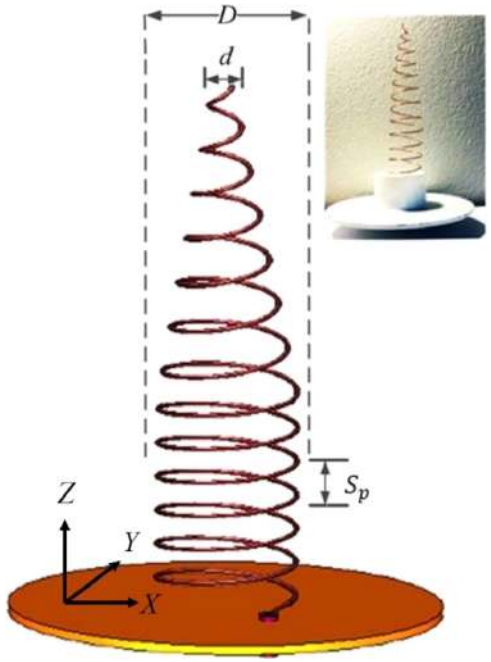

FIG. 3. The quasi-conical spiral structure (left) and the photograph of the antenna (right).

electric field for illumination. We also show the electric field distribution at the distance of 10 cm. Figure 5(g) shows the electric field distribution along the line of x = 7.5 cm. Curves (a–d) correspond to Figs. 5(a)–5(d). Comparing the traditional helical antenna, the quasi-conical spiral antenna can produce a more uniform electric field. The electric distribution along the Z axis is shown in Figs. 5(e) and 5(f). The directivity of the traditional helical antenna is better than that of the quasi-conical spiral antenna. A high local electric field can be achieved on one hand. However, on the other hand, undesired nonhomogeneous electric fields are always generated in the testing domain.[29] For thermoacoustic imaging, the electric field density generated by the quasi-conical spiral antenna is strong enough to achieve a high signal noise ratio (SNR) at the distance of 5 cm. Therefore, we prefer to place the object close to the antenna when the electric field is relatively uniform within the field of view. The disadvantage of the quasi-conical antenna is the limitation in power capacity. However, coupled with a microwave source (60-kW peak power), the power emitted by the antenna was adequate to image biological tissues. The comparison between different types of antennas in TAT is shown in Table I.

We designed a phantom to demonstrate the specific absorption rate (SAR) distribution under the illumination of different antennas. The phantom used in the simulation was a dielectrically homogeneous cylinder with a relative permittivity of 70 and a conductivity of 2.0 S/m, which is close to

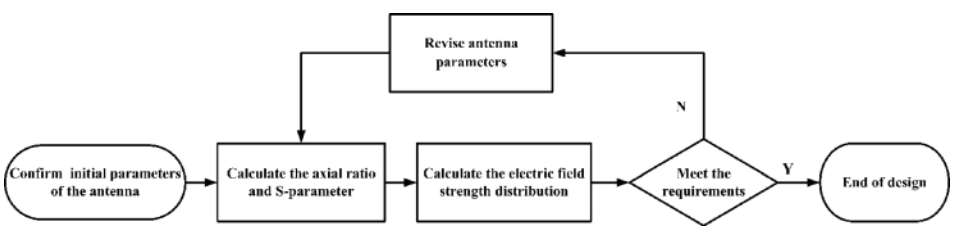

FIG. 2. The flow chart of the antenna design process.

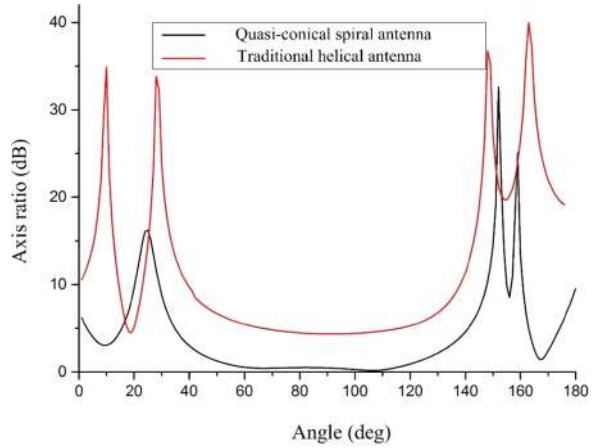

FIG. 4. The axial ratio of the antenna.

the dielectric properties of breast tumors.[30] The phantom is a dielectrically homogenous cylinder with a 10-mm diameter and a 10-mm length. The phantom was placed 5 and 10 cm above the antenna and was imaged at three locations with different distances from the center [Fig. 7(b)]. The SAR distribution in the phantoms produced by antenna is shown in Fig. 6. The SAR boundary distribution of the phantom is of great importance in imaging. As we can see from the figure, the phantom will be more homogeneously illuminated with circularly polarized microwaves by using the quasi-conical spiral antenna. The microwave energy dissipation outside the phantom is highly homogenous with maximum values located close to the boundary of the phantom, while the microwave energy dissipation inside the phantom is relatively small. On the other hand, for the traditional helical antenna, the microwave energy dissipation inside the cylinder is nonuniform. The distribution has a "splitting" pattern with greater SAR values located near the boundaries intersecting with the $\hat{x}$ direction, which happens to be the elliptical polarization. However, the electric field density is not strong enough for high signal noise ratio (SNR) testing at the distance of 10 cm with a 60 kW peak-power source. We conduct the experiment at the distance of 5 cm.

The experimental setup is shown in Fig. 7(a). The microwave source generated a peak power of 60 kW and illuminated the phantoms from the bottom. The microwave pulse width was 0.6 μs, and the pulse repetition rate was 10 Hz. The phantom was made of 3% agar powder and 97% water to mimic breast tissue.[31] We immersed the phantom in a container filled with mineral oil for acoustic coupling. An ultrasonic transducer (V323, Panametrics-NDT, 2.25-MHz central frequency, and 6-mm diameter) was fixed on a rotational scanner. The transducer and data cables were shielded with a metal mesh to reduce microwave interference. The generated thermoacoustic signals received by the transducer

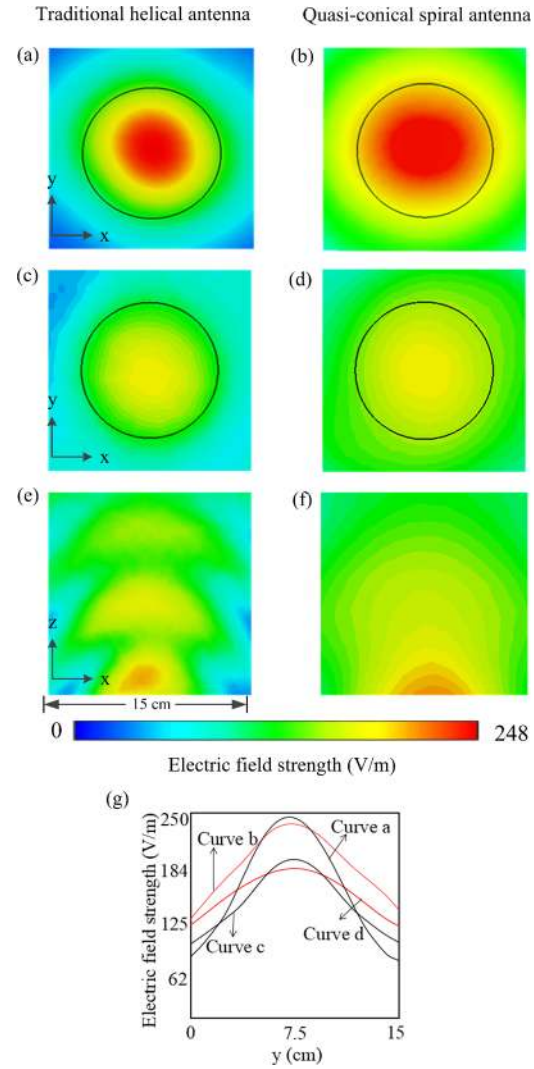

FIG. 5. Simulated distribution of the electric field produced by the traditional helical antenna [(a), (c), and (e)] and the quasi-conical spiral antenna [(b), (d), and (f)]. (a) and (b) The x-y cross section images at the distance of 5 cm. (c) and (d) The x-y cross section images at the distance of 10 cm. (e) and (f) The images along the z-axis from the distance 0 cm to 10 cm. (g) The electric field distribution along the line of x = 7.5 cm.

was first amplified by a low noise amplifier followed by a 40-dB amplifier (5072PR, Panametrics) and then recorded by a data-acquisition (DAQ) card with a sampling frequency of 20 MHz. The transducer was scanned around the phantom for 800 steps, and the signals were averaged 30 times. We reconstructed TAT images using a back-projection algorithm.[32]

Under the same experimental circumstance, we tested two antennas working at 3 GHz to demonstrate the effect of the antennas on the reconstructed images. The phantoms are dielectrically homogenous cylinders with 10-mm diameters and 10-mm lengths. The phantom was placed 5 cm above the antenna and was imaged at three locations with different

TABLE I. The comparison between different types of antennas in TAT.

	Power capacity	Polarization	Size	Uniform electric field region
Horn antenna	Large	Linear polarization	Large	Medium
Traditional helical antenna	Medium	elliptical polarization	Small	Small
Quasi-conical spiral antenna	Medium	circular polarization	Small	Large

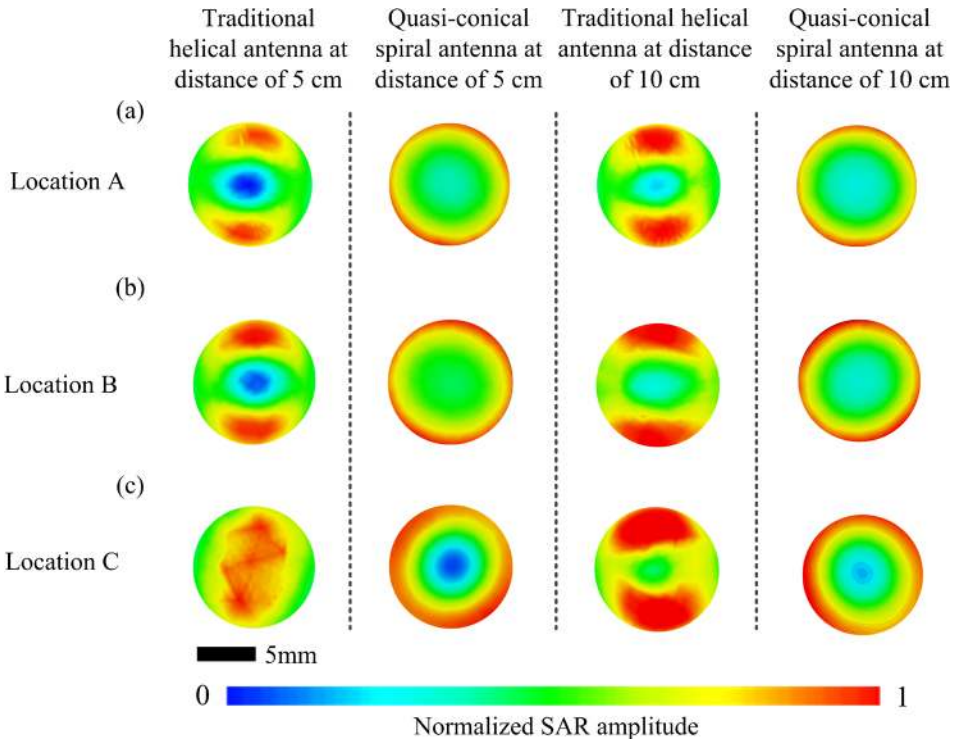

FIG. 6. The SAR distribution of the phantom at (a) location A, (b) location B, and (c) location C indicated in Fig. 7(b). The first and second rows show the SAR distribution images at the distance of 5 cm by the traditional helical antenna. The third and fourth rows show the SAR distribution images at the distance of 10 cm.

distances from the scanning center [Fig. 7(b)]. The images produced by the traditional helical antenna are shown in the left panel of Fig. 8. The simulated SAR distribution (first row in Fig. 6) is consistent with the reconstructed image (left row of Fig. 8). We can see "splitting" distortions caused by the linear components of the electric field. For the phantom, simulated SAR at location C does not demonstrate the "splitting" pattern indicated in Fig. 8 by using the traditional helical antenna. We suspected that the splitting behavior was induced by the standing wave formed in the phantom, and the antinodes can be observed at the center and at the edge, with the maximum values located in the center region. The SNR for location A, location B, and location C is 21, 13, and 7. We then changed the antenna to the quasi-conical spiral antenna, and the images of the phantom at the same locations are shown in the right panel of Fig. 8. The spurious features in the images are significantly reduced. The SNR for location A, location B, and location C is 19, 15, and 13. Comparing the images acquired with different antennas (horizontal comparison), we conclude that the quasi-conical spiral antenna can provide a higher circularly polarized electric field. We further compare the images of the phantom at different locations (longitudinal comparison). The "splitting" distortions are more obvious when the phantom is moved away from the scanning center. However, because the quasi-conical spiral antenna can produce a larger radiation field with uniform illumination, the spurious features in the images increase more slowly when the phantom is moved away from the center. For the quasi-conical spiral antenna, the radiation angle is out of the range of the low axial ratio (60°–120°) when the phantom was placed at locations B and C (Fig. 4). An ellipse polarization of the electric field caused the "ring" features. However, the phantom in the image produced by the quasi-conical spiral antenna was not split as that produced by the

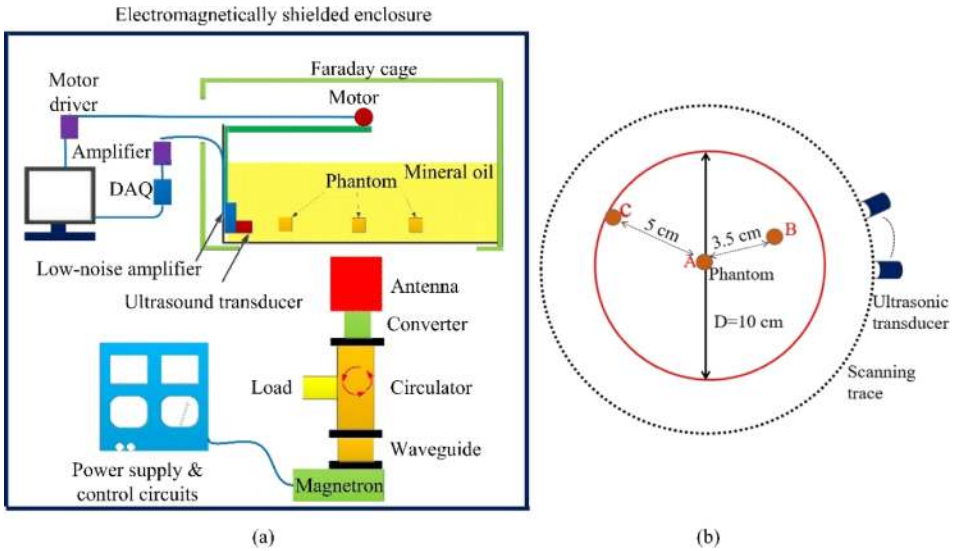

FIG. 7. (a) Experimental setup. DAQ, data acquisition circuits. (b) Top view of the scanning configuration.

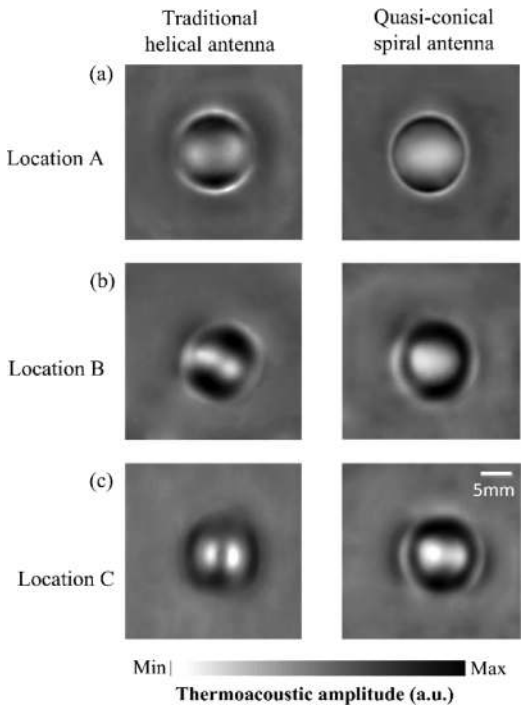

FIG. 8. The reconstructed images of the phantom at (a) location A, (b) location B, and (c) location C indicated in Fig. 7(b). The left row shows the images produced by the traditional helical antenna. The right row shows the images produced by the quasi-conical spiral antenna.

helical antenna [Figs. 8(b) and 8(c)]. We can also clearly identify the target. For the phantom under the traditional helical antenna illuminating, the "splitting" pattern may lead to false imaging.

In summary, we propose a quasi-conical spiral antenna for TAT. Compared to the traditional helical antenna commonly used in TAT, the proposed antenna realized circular polarizations. It significantly eliminates "splitting" distortion and provides a larger uniform electric field for illumination. These advantages enable the proposed antenna to improve the image quality, which is expected to benefit clinical imaging. For example, the quasi-conical spiral antenna can potentially be coupled with an ultrasonic transducer array to detect breast cancer.

This work was supported in part by the China 973 program and the China Scholarship Council.

[1]L. M. Neira, B. D. Van Veen, and S. C. Hagness, IEEE Trans. Antennas Propag. **65**(11), 6002 (2017).
[2]E. C. Fear, Technol. Cancer Res. Treat. **4**(1), 69–82 (2005).
[3]J. D. Shea, P. Kosmas, S. C. Hagness, and D. B. Van Veen, IOP Ltd, Jun. 2010
[4]G. Ku, B. D. Fornage, X. Jin, M. H. Xu, K. K. Hunt, and L. V. Wang, Technol. Cancer Res. Treat. **4**(5), 559–565 (2005).
[5]M. Pramanik, G. Ku, C. H. Li, and L. V. Wang, Med. Phys. **35**(6), 2218–2223 (2008).
[6]R. A. Kruger, P. Liu, Y. R. Fang, and C. R. Appledorn, Med. Phys. **22**, 1605–1609 (1995).
[7]A. Karabutov, E. V. Savateeva, N. B. Podymova, and A. A. Oraevsky, J. Appl. Phys. **87**, 2003–2014 (2000).
[8]W. Ding, Z. Ji, and D. Xing, Appl. Phys. Lett. **110**(18), 183701 (2017).
[9]F. Gao, Y. J. Zheng, and D. F. Wang, Appl. Phys. Lett. **101**, 043702 (2012).
[10]P. M. Meaney, K. D. Paulsen, and J. T. Chang, IEEE Trans. Microwave Theory Tech. **46**, 31–45 (1998).
[11]L. M. Zeng, D. Xing, H. M. Gu, D. W. Yang, S. H. Yang, and L. Zh. Xiang, Chin. Phys. **23**, 1215 (2006).
[12]D. Feng, Y. Xu, G. Ku, and L. V. Wang, Med. Phys. **28**(12), 2427–2431 (2001).
[13]Y. He, C. Liu, L. Lin, and L. Wang, IEEE Antennas Wireless Propag. Lett. **16**, 1593–1596 (2017).
[14]Yu. A. Andreev, A. M. Efremov, V. I. Koshelev, B. M. Kovalchuk, A. A. Petkun, K. N. Sukhushin, and M. Yu. Zorkaltseva, Rev. Sci. Instrum. **85**, 104703 (2014).
[15]A. Mashal, J. H. Booske, and S. C. Hagness, Phys. Med. Biol. **54**(3), 641 (2009).
[16]D. R. Bauer, X. Wang, J. Vollin, H. Xin, and R. S. Witte, Appl. Phys. Lett. **101**, 033705 (2012).
[17]H. Ke, T. N. Erpelding, L. Jankovic, C. Liu, and L. V. Wang, J. Biomed. Opt. **17**(5), 056010 (2012).
[18]L. Huang, L. Yao, L. Liu, J. Rong, and H. Jiang, Appl. Phys. Lett. **101**(24), 244106 (2012).
[19]D. Yang, D. Xing, H. Gu, Y. Tan, and L. Zeng, Appl. Phys. Lett. **87**, 194101 (2005).
[20]C. Li, M. Pramanik, G. Ku, and L. V. Wang, Phys. Rev. E **77**(3), 031923 (2008).
[21]Y. He, Y. Shen, X. Feng, C. Liu, and L. V. Wang, Appl. Phys. Lett. **111**, 063703 (2017).
[22]L. H. V. Wang, X. M. Zhao, H. T. Sun, and G. Ku, Rev. Sci. Instrum. **70**, 3744 (1999).
[23]A. J. Ernest, Y. Tawk, J. Costantine, and C. G. Christodoulou, IEEE Trans. Antennas Propag. **63**(1), 41–47 (2015).
[24]C. W. Penney and R. J. Luebbers, IEEE Trans. Antennas Propag. **42**(9), 1328 (1994).
[25]G. Biffi Gentili, M. Cerretelli, and L. Cecchi, **18**(1), 85–97 (2004).
[26]V. H. Rumsey, *Frequency Independent Antennas* (Academic Press, New York, 1966).
[27]J. Thaysen, K. B. Jakbsen, and J. A. Hansen, Appl. Microwave Wireless **13**(2), 32–45 (2001).
[28]H. Nakano, Y. Samada, and J. Yamauchi, IEEE Trans. Antennas Propag. **34**, 1143–1148 (1986).
[29]C. A. Balanis, Proc. IEEE **80**(1), 7 (1992).
[30]M. Lazebnik, L. McCartney, D. Popovic, C. B. Watkins, M. J. Lindstrom, J. Harter, S. Sewall, A. Magliocco, J. H. Booske, M. Okoniewski, and S. C. Hagness, Phys. Med. Biol. **52**, 2637–2656 (2007).
[31]K. Mannickam, M. R. Reddy, S. Seshadri, and B. Raghavan, J. Med. Imaging) **2**(4), 047002 (2015).
[32]M. H. Xu and L. H. V. Wang, IEEE Trans. Med. Imaging **21**(7), 814 (2002).